ACS NANO

www.acsnano.org

ARTICLE

Quantum Confinement in Epitaxial Armchair Graphene Nanoribbons on SiC Sidewalls

Thi Thuy Nhung Nguyen, Stephen R. Power,* Hrag Karakachian, Ulrich Starke, and Christoph Tegenkamp*

Cite This: *ACS Nano* 2023, 17, 20345−20352

Read Online

ACCESS | Metrics & More | Article Recommendations

ABSTRACT: The integration of graphene into devices necessitates large-scale growth and precise nanostructuring. Epitaxial growth of graphene on SiC surfaces offers a solution by enabling both simultaneous and targeted realization of quantum structures. We investigated the impact of local variations in the width and edge termination of armchair graphene nanoribbons (AGNRs) on quantum confinement effects using scanning tunneling microscopy and spectroscopy (STM, STS), along with density-functional tight-binding (DFTB) calculations. AGNRs were grown as an ensemble on refaceted sidewalls of SiC mesas with adjacent AGNRs separated by SiC(0001) terraces hosting a buffer layer seamlessly connected to the AGNRs. Energy band gaps measured by STS at the centers of ribbons of different widths align with theoretical expectations, indicating that hybridization of π-electrons with the SiC substrate mimics sharp electronic edges. However, regardless of the ribbon width, band gaps near the edges of AGNRs are significantly reduced. DFTB calculations successfully replicate this effect by considering the role of edge passivation, while strain or electric fields do not account for the observed effect. Unlike idealized nanoribbons with uniform hydrogen passivation, AGNRs on SiC sidewalls generate additional energy bands with non-p_z character and nonuniform distribution across the nanoribbon. In AGNRs terminated with Si, these additional states occur at the conduction band edge and rapidly decay into the bulk of the ribbon. This agrees with our experimental findings, demonstrating that edge passivation is crucial in determining the local electronic properties of epitaxial nanoribbons.

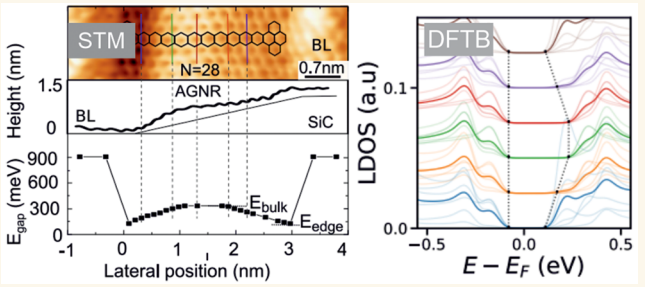

KEYWORDS: *graphene nanoribbons, edge termination, band gaps, tight-binding simulations, scanning tunneling microscopy*

INTRODUCTION

Graphene nanoribbons (GNRs) are attractive building blocks for carbon-based electronics and even suitable for quantum electronics.[1] Similar to carbon nanotubes,[2−4] graphene ribbons have been shown to provide ballistic and semiconducting channels.[5−8] However, here the edges play a crucial role but, at the same time, offer the possibility for the synthesis of other quantum phases after further functionalization.[9−11]

GNRs of different chirality, ribbon widths, edge orientations, and edge terminations have been realized by means of an on-surface synthesis with molecular precursors on metallic supports.[11−15] Targeted modification of the band structure has been achieved, e.g., by placing specific atoms at predesigned locations.[16−19] In general, the functionalization of the edges of GNRs is a promising strategy and allows further tuning of the electronic and optical properties.[20,21] This often involves the modification of band gaps of the entire ribbon as well as the synthesis of edge states and topological phases.[22] Furthermore, based on edge functionalization schemes, the fabrication of macromolecular networks succeeds and offers the possibility to grow polymers with sophisticated topologies.[23]

Large-area and scalable GNR arrays can be fabricated directly on insulating SiC substrates with appropriate mesas by high-temperature annealing, eliminating the need for subsequent transfer techniques.[24,25] Thereby, the width and edge topology of the GNRs is tunable and defined by the SiC-mesas and allows the growth of both gapped armchair and ballistic zigzag GNRs due to confinement and hybridization of the edges, respectively.[8,26,27]

Received: July 13, 2023
Accepted: September 29, 2023
Published: October 3, 2023

Armchair graphene nanoribbons (AGNRs) provide a large flexibility and are either metallic or semiconducting depending on the number N of sp^2 hybridized C atoms across the ribbon. In a recent photoemission experiment the formation of one-dimensional (1D) confined AGNRs was demonstrated.[8] The average ribbon width was around 2 nm, and all features of the measured two-dimensional (2D) band structure of an ensemble of around 500 AGNRs were consistent with 1D confinement effects, assuming AGNRs with mainly three different widths N = 16, 18, 20. Compared to the on-surface synthesized AGNRs, the epitaxial ribbons on SiC supports are different as seen by scanning tunneling microscopy:[25,26] the instability of the SiC sidewall running along the [11$\bar{2}$0] -direction and which are on average inclined by approximately 27° comes along with step bunching resulting in the formation of small stripes of SiC(0001) terraces of 1 nm in width. As a consequence, the p_z states of the selectively grown graphene get saturated from the dangling bonds of the Si-terminated SiC(0001) terraces forming stripes of buffer layers (BLs) with sp^3-like hybridized C atoms with suspended AGNRs in between.[25,28] Therefore, quantum confinement is achieved here not by a sharp edge or by hydrogen-passivation but by the bonds formed between the edge atoms of the AGNRs with the substrate or the BL. This different edge scenario should affect the bonding distances as well as breaking the uniform p_z character of low-energy electronic states in the system.

In this work, we have performed a detailed analysis of the band gaps of epitaxial AGNRs using both STM measurements and theoretical modeling. Band gap measurements show a robust decrease in gap magnitude as we move away from the center of a ribbon toward the edges. While environmental factors like strain or electric fields can tune the global band gap, we find that they are not sufficient to induce this spatial variation of the band gap. Instead, our calculations show that passivation effects are required to introduce the edge localized states responsible for the varying gap size and apparent pinning of the valence band edge. In particular, a simple passivation with Si atoms is found to excellently reproduce the variation in the gap sizes found experimentally. This suggests that edge passivation effects in epitaxial GNRs play a crucial role in determining their electronic structure and, in particular, that states induced by dangling bonds or hybridization with termination species can dominate behavior near the band edges.

RESULTS AND DISCUSSION

Growth of Epitaxial AGNRs on SiC Sidewalls. Epitaxial armchair graphene nanoribbons (AGNRs) were grown on the sidewalls of SiC mesas running along the ⟨11$\bar{2}$0⟩ direction, as shown by the large-scale STM image in Figure 1a. Similarly to zigzag-type GNRs grown on perpendicularly aligned SiC mesas,[27] the GNR grows selectively and carpets over the entire sidewall structure of around 40 nm. Contrary to the zigzag-GNRs, the SiC facet for the AGNR decomposes further upon high-temperature annealing and forms mini SiC(0001) terraces, as sketched in Figure 1c.[25] As demonstrated by high-resolution low-energy electron diffraction experiments, adjacent mini-terraces are separated by a full polytype unit cell, i.e., six SiC bilayers.[8] The periodicity of the washboard structure (Figure 1b) is around 3.1 nm, and the AGNRs provide on average a width of around 2.1 nm (i.e., N = 18 AGNR) in agreement with previous studies.[26] This one-

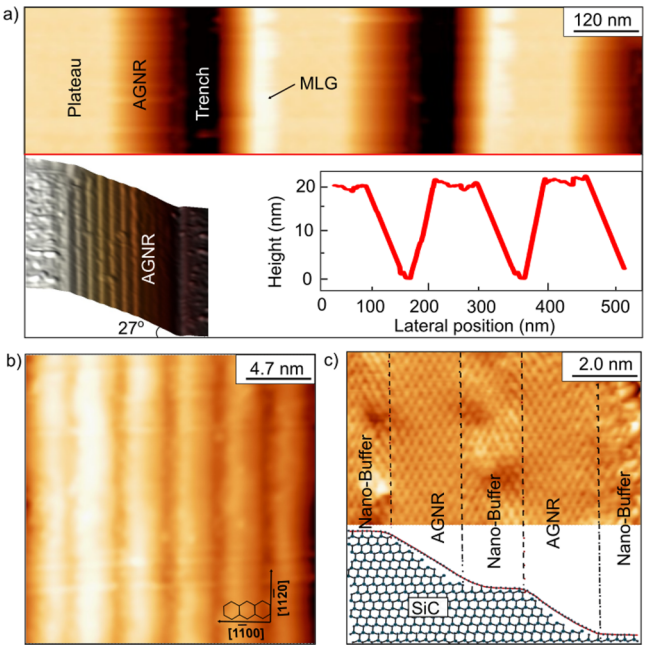

Figure 1. Selective growth of epitaxial AGNR on the sidewalls of SiC mesas. (a) STM image of SiC mesa structures along the [11$\bar{2}$0] direction revealing AGNR ensembles on each of the sidewalls between the plateaus and trenches (+2 V, 0.5 nA). From the 3D STM image (−1 V, 0.5 nA) the inclination of the sidewalls of 27° is visible. The height profile taken across the mesas shows the pitch size and height of 200 and 20 nm, respectively. The edges of the plateaus were slightly overgrown with a monolayer graphene (MLG). (b) Zoom-in of an AGNR ensemble (−1 V, 0.5 nA) showing a washboard-like structure on a sidewall. (c) STM image with atomic resolution (−2 V, 0.5 nA) distinguishes the semiconducting nanobuffer layers and free-standing AGNR on the nanofacets. Bottom: side-view schematic of the AGNR formation on the refaceted SiC sidewall. On average, the AGNR and nanobuffer areas reveal widths of 2 and 1.1 nm, respectively.

dimensional confinement gives rise to robust quantization and formation of subbands, as seen by recent angle-resolved photoemission spectroscopy (ARPES) measurements.[8]

Despite the outstanding homogeneity, which we achieved, the facets reveal partly irregularities and the local variation of the widths manifests with the observation of metallic and semiconducting bands.[8] Moreover, compared to GNR structures synthesized by on-surface chemistry where the in-plane σ-bonds are saturated with hydrogen,[11,15] the edges of the AGNRs in this study are defined by the BL stripes, i.e., by bonds of the π-electrons with the dangling bonds of the Si-terminated surface. Both effects come inevitably along with a variation of the width; thus, these AGNRs are perfectly suited to study the effect of edge termination and variation of width toward the quantum confinement. For the zigzag GNRs (ZGNRs), we have recently shown that electric field defects of the SiC surface also play a role and explain, among other things, the spatial separation of the volume transport channels.[7] However, for these ribbons, one of the edges merges perpendicularly into the SiC face.[27] For the AGNRs here, the edge bonding scenario is different and beyond and also symmetric. As we will show in addition, electrostatic potential effects alone do not lead to a significant spatial segregation of electronic states or variations in measured quantities, such as the local band gap. Rather, the bonds of the

https://doi.org/10.1021/acsnano.3c06449
ACS Nano 2023, 17, 20345−20352

C atoms to the Si surface atoms are decisive for the epitaxial system.

Quantum Confinement and Band Gap Opening. The formation of edges by saturation of the p_z orbitals and, concomitantly, opening of band gaps is shown in Figure 2.

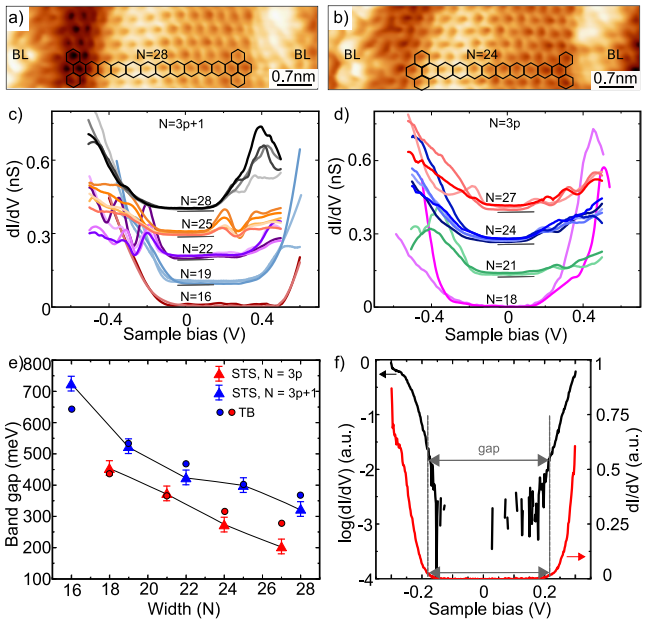

Figure 2. Width dependence of the bulk energy gaps. (a, b) High-resolution STM images (+2.0 V, 0.5 nA) for two AGNRs from the semiconducting 3p (N = 24) and 3p+1 (N = 28) families. (c, d) STS-spectra taken in the center of various AGNRs of different widths for semiconducting 3p and 3p+1. The spectra shifted for better visibility. (e) Band gaps for various semiconducting AGNRS determined by STS and TB (circles). (f) Semilog and linear plot of the dI/dV spectra to show the determination of the gap energies, exemplarily for an N = 25 AGNR.

Panels (a) and (b) show sections of N = 28 and N = 24 ribbons, belonging to the semiconducting 3p+1 and 3p families, respectively, with comparatively straight edges. For clarity, we overlaid a hexagonal grid to highlight the ribbon width and the armchair direction of the edges. The scanning tunneling spectroscopy (STS) spectra shown in panels (c) and (d) are taken at the centers of a range of similar structures and clearly show an increasing energy gap with decreasing widths. The evolution of the band gap with ribbon width, from N = 16 to N = 28, is plotted in Figure 2e, where the individual gap values were determined using both linear and semilog plots of the dI/dV data (cf. panel f). These gap energies are in good agreement with those extracted from tight-binding (TB) band structures (circular symbols in Figure 2e) and also with the results of first-principle calculations using the local density approximation (LDA).[20] We note that these theoretical models consider perfect, H-passivated edges, whereas in our experiment, the ribbons are terminated by the hybridization with atoms in the BL regions or the underlying SiC substrate. The reasonable agreement with our TB simulations of finite-width ribbons suggests that a perturbation of the sp^2 hybridization is sufficient to induce a robust quantization and the associated band gap trends in AGNRs.

The AGNRs investigated here are all charge-neutral; i.e., the Fermi energy lies within the band gap of the ribbons, in agreement with previous experiments.[8,26] Moreover, close inspection of Figure 2c shows also that the valence band for many of the AGNRs is pinned approximately 0.1 eV below the Fermi energy. This pinning is particularly evident for the GNRs of the N = 3p+1 family (Figure 2c). For the N = 3p ribbons the pinning is less clear. For AGNRs on Au(111) a similar Fermi level pinning was found for ribbons with band gaps lower than 1.7 eV.[29] For this system, the authors propose that metal-induced bandgap states prevent pushing of the AGNR valence band above the Fermi energy. Such an explanation is maybe not appropriate for our purely semiconducting system consisting of the AGNR quantum well states, the BL, and the SiC crystal. Instead, the apparent pinning in our system suggests the presence of states whose energy is not strongly dependent on the width of the ribbon, i.e., states arising not from confinement effects but from the specifics of the edge-substrate interaction.

Variation of Gap Energies: Role of Edge Termination. The benchmarking of the experimentally determined band gaps with the results of the simple TB model succeeds when the energy gaps are determined at the center of ribbon segments, which are terminated by straight edges. In Figure 3a

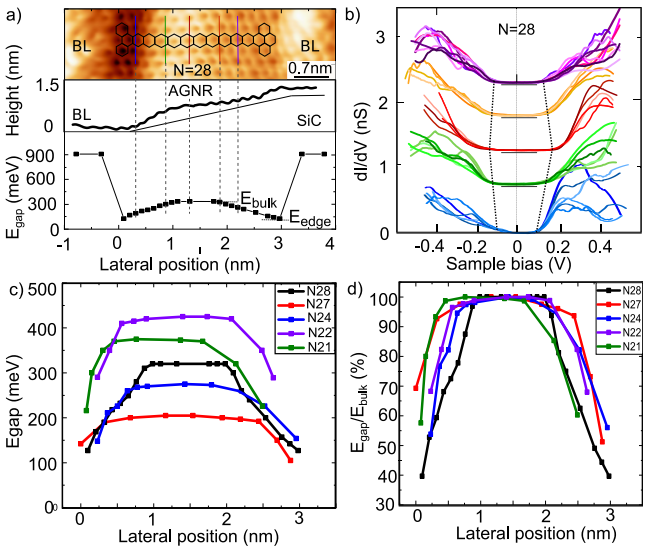

Figure 3. Spatial variation of the energy band gaps. (a) Variation of the energy gap across an N = 28 AGNR. (top) STM image and line profile were spectroscopy was performed. (b) dI/dV spectra along the ribbon at various positions across the ribbon. The colors refer to those in panel (a). The spectra are shifted for better visibility. (c) Variation of energy gaps for various AGNRs as a function of the position across the ribbon. (d) Renormalized gap energies of (c) revealing a universal behavior.

we plot the structure, height profile, and energy gaps found for an N = 28 AGNR (width of 3.3 nm) with respect to the lateral position across the AGNR. These results show a clear variation in the magnitude of the band gap across the width of the ribbon, characterized by a considerable reduction in gap size near the ribbon edges, before an abrupt jump to approximately 900 meV, which resembles the gap size previously reported for the BL.[30] Examples of the individual STS curves used to determine the band gaps are shown in Figure 3b. To remove possible effects due to local defects, we measured multiple spectra over a range of 1 nm along the ribbon direction for each of the different possible lateral positions across the ribbon width. These are shown by the similarly colored curves in

https://doi.org/10.1021/acsnano.3c06449
ACS Nano 2023, 17, 20345−20352

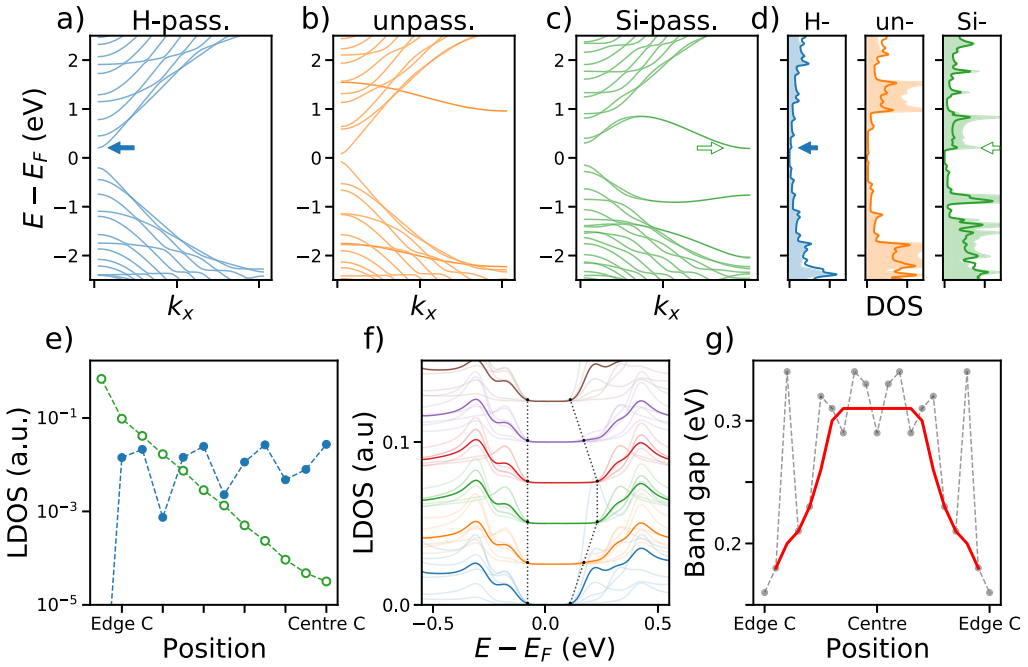

Figure 4. Passivation effects on states and band gaps. (a−c) Comparison of the band structures from DFTB calculations for a 21-AGNR with H-passivated edges, unpassivated edges, and Si-passivated edges, respectively. (d) The densities of states (per atom) for each of the conditions considered, with the solid lines showing the total DOS and the shaded regions showing the contribution from the edge region (three carbon atoms nearest the edge together with the passivating atom). (e) LDOS at the upper band edge (shown by arrows in upper panels) for H-passivated (filled, blue circles) and Si-passivated (open, green circles) ribbons as a function of position from the edge. (f) LDOS at different positions across the Si-terminated ribbon width, from one edge (bottom, blue curve) to the opposite edge (top, brown curve). The bold lines represent the averaging of the spectra calculated on nonequivalent C atoms across the ribbon. (g) The band gap extracted from the LDOS as a function of position from the Si-terminated ribbons. The black curve shows results for individual atoms, with the bold red curve averaging over three sites to remove the short-ranged oscillations.

Figure 3b, with the curves for each lateral position showing very similar trends and almost identical band gap values. In this region, the edges were parallel, and the bulk spectra show no change in band gap at the center of the ribbon. The typical gap size value for the $N = 28$ AGNR, as found at the center of the ribbon, is about 320 meV, which agrees well with previous studies.[8,20,25] The band gaps in the center of the ribbon are therefore consistent with those expected from a simple 1D confinement, whereas the reduced energy gaps observed near the ribbon edges deviate from the expected trend and must originate from the nature of the edges themselves.

The areas next to the AGNRs, as marked by BL in Figure 3a (cf. also Figure 1c), have a gap consistent or at least close to values reported for the BL[30,31] and support the formation of wide band gap BL stripes, which decouple adjacent ribbons. Previous work has also reported the formation of armchair miniribbons on the SiC sidewalls, but these are separated by so-called pinning regions.[26] While these AGNRs have clear and comparable band gaps to ours, the pinning areas have a finite density of states at E_F and are metallic. In contrast to our work, the formation of the AGNRs was found essentially at the top and bottom edges of the sidewall, while for the 6H-SiC polytype and other heating protocols used in our work, we obtained a much more homogeneous size and spacing distribution, which apparently have led to the formation of insulating structures between the AGNRs. The jump in band gap size to the BL value occurs essentially within a single graphene unit cell, demonstrating that the edges of our epitaxial AGNRs are atomically sharp. As there is a seamless connection between the free-standing graphene ribbon and the BL, the edges are defined by the hybridization of the p_z orbitals with the dangling bonds of the Si atoms on the SiC(0001) surface.

The variation of the gap size across the ribbons is a generic feature and was found for all of the ribbons investigated here. The variation of gap size with lateral position is shown for a variety of AGNRs with different widths in Figure 3c. As can be seen, the central part of each AGNR studied has a constant band gap, E_{gap}, extending over approximately 60−70% of the total ribbon width. Toward the ribbon edges, the band gap drops significantly to about half of the bulk gap value. The qualitative trend is independent of the width of the ribbons, as the plot in panel (d) highlights. This decrease of the expected band gap in the direction of the edges seems to be characteristic for our epitaxial AGNRs. Fortunately, for device applications, the fact that the band gap is not fully quenched at the edge still allows for a range of electronic applications with this material system. Similarly, the transition to the BL presents a quasi-atomically sharp transition and allows robust quantization, so that epitaxial AGNRs indeed act as one-dimensional quantum systems. However, the effective ribbon band gaps deviate significantly from expected theoretical values, and this deviation can be easily missed if, for example, the ribbons are characterized solely by STS measurements at the ribbon centers. It is therefore crucial to understand the mechanisms behind the band gap renormalization, both from fundamental science and device design perspectives.

To explain the spatial variation of the measured band gaps across AGNRs on SiC, several mechanisms can be considered: as Figure 3a shows, the AGNRs are slightly concavely curved,

https://doi.org/10.1021/acsnano.3c06449
ACS Nano 2023, 17, 20345−20352

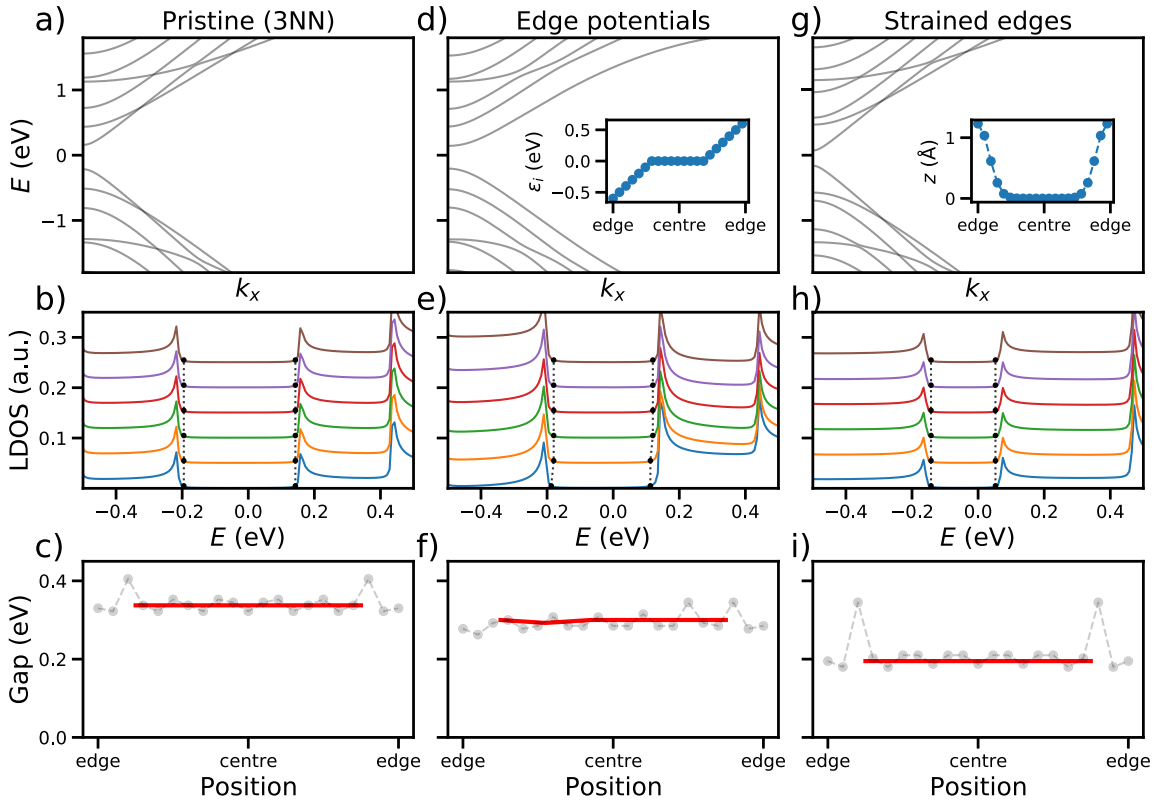

Figure 5. Local potential and strain effects. Tight-binding results for a pristine (left), transversely biased (middle), and strained 21-AGNR (right). For each of the bands (top), LDOS at various points across the ribbon (middle) and gap vs position (bottom) are shown. The right hand side will show the structure of an edge-disordered ribbon (top), together with gap profiles along (top) and across (bottom) the ribbon.

which can be associated with strain effects.[32] Furthermore, similar to the AGNR/Au(111) system, charge transfer is also possible, which leads to the formation of dipole moments or electrostatic fields.[29] In the next section, we show that none of these scenarios lead to the peculiar position dependence observed in our experiments.

Instead we propose here that the experimental findings are consistent with the formation of additional edge-localized states, which arise due to the nonstandard passivation of epitaxial AGNR edges. Free-standing epitaxial AGNRs merge with BL stripes whose carbon atoms in turn interact with Si atoms on the SiC surface, to which the BL is bound. Although the exact atomic configuration is not known, in Figure 4 we examine some simplified cases which highlight the range of effects which result from different passivation scenarios via in-plane σ-bonds. The DFTB-calculated band structures of a 21-AGNR with H-passivated, unpassivated, and Si-passivated edges are shown in panels (a−c). We note that a simple hydrogen passivation of the edges results in a band structure in excellent agreement with a perfect one-dimensional quantization of graphene's two-dimensional dispersion. This is the case regardless of whether the hydrogen atoms are explicitly included, as in the DFTB bands here, or implicitly within a TB calculation as shown later in Figure 5a. Unlike ZGNRs, which have distinctive edge states at the Fermi energy, the electronic states of AGNRs are evenly distributed across the ribbon width. This can be seen in Figure 4d, where the density of states (per atom) of the entire ribbon, shown by the solid blue curve, matches almost exactly with the same quantity taken only near the edge (shaded area). This is also clear from the blue curve in Figure 4e, which plots the local density of states (LDOS), in log scale, projected onto each atom from the edge to the center of the ribbon. The LDOS is calculated at an energy near the conduction band edge, shown by the blue arrow in panels (a) and (d). Aside from a very short-ranged oscillation, with a 3-atom period characteristic of quantities measured along the zigzag direction,[33] the distribution of this state is uniform across the ribbon. As discussed below, this uniformity is very difficult to break within simple TB models.

Removing the passivating atom altogether introduces a distinctive band, clearly visible in Figure 4b. This forms due to coupling between dangling-bond states at the unpassivated carbon edge sites and has a non-p_z character that is not captured by TB simulations.[34,35] This state resides at the ribbon edge and results in an enhanced density of states near the edge of the ribbon (shaded orange area in panel d). However, at this ribbon width this state is further from the Fermi energy than the first few confinement-induced subbands and so will not directly influence band gap measurements. This changes, however, if we consider passivation by other atomic species where more complicated hybridization can occur. In particular, the passivation of the edges with Si atoms reveals a state in the vicinity of the band gap, as highlighted by the green arrow in Figure 4c. Similar to the unpassivated system, this state is edge-localized and enhances the density of states near the ribbon edge (shaded green area in panel d). This is shown more explicitly by the green curve in Figure 4e, which confirms that the state decays exponentially toward the center of the ribbon. The presence of an edge-localized state at the band edge suggests that STS band gap measurements will be strongly affected by the position of the

https://doi.org/10.1021/acsnano.3c06449
ACS Nano 2023, 17, 20345−20352

probe and, in particular, the extent to which it samples the edge-localized states.

In Figure 4f we show the LDOS at different positions across the ribbon width. To account for the finite size of the probe, the bold curves presented here are averaged over 6 nearby, nonequivalent sites, whose individual spectra are shown by lighter curves of the same color. The different sets of curves have a relative shift for clarity, with the top and bottom sets representing opposite sides of the ribbon. The evolution of the band edges is shown by black dotted lines and is in good agreement with the experimental data shown in Figure 3b. Finally, the band gap values extracted from the local density of states as a function of position are plotted in panel (g). The gray, dashed curve shows results for individual atoms and again displays the characteristic period-3 oscillation. The bold red curve averages over three sites to remove this artifact, and its behavior is in excellent agreement with the experimental curves in Figure 3c, showing a similar band gap reduction as we move from the center to either edge of the ribbon.

Further Environmental Effects. As already mentioned, there are other environmental effects that could possibly also lead to spatial variation of the band gaps. Previous studies found that local variations in potential[7] or strain[27] were key to explaining unexpected quantum transport or spectroscopic signatures in epitaxial ZGNR structures on SiC sidewalls. In particular, transverse field effects lead to a spatial segregation of states in these systems and can be captured within a TB model using position-dependent on-site energy terms ϵ_i. It is reasonable to expect that a similar effect could emerge in AGNRs. Similarly, by varying hopping terms in different parts of the ribbon,[36] inhomogeneous strain could also act to break the uniform distribution of states typically expected for AGNR systems.

The consideration of additional potential or strain effects is also justified by the experimental conditions. As shown in the context of Figure 3a,b, there is an atomically sharp boundary between the BL and the AGNR which resembles a type-1 semiconductor heterostructure, in agreement with our STM results concerning the band gaps and the positions of the valence and conduction bands. Furthermore, relying on the work functions measured for buffer layer graphene (3.9 eV) and quasi-free-standing graphene (4.8 eV),[37] electric fields of 0.5−1 V/nm can be formed symmetrically at both boundaries. Indeed, in-plane electric-field modulation effects have already been observed for free-standing AGNRs[38] where at least for larger ribbons ($N > 18$) a significant reduction of the band gap was found for fields exceeding 0.7 eV/nm. However, it is the global band gap which varies, and the effect depends sensitively on the ribbon width and electric field. Furthermore, as sketched in Figure 1c, the AGNRs result from the formation of mini-SiC(0001) terraces upon annealing of the SiC mesa structure. Due to this growth mode, strain effects are unavoidably involved as also apparent from the line height profile shown in Figure 3a. It has previously been shown that band gaps in H- or O-passivated AGNRs can be quenched by applying tensile strain in the order of 12%.[39] Indeed, a small compressive strain on the edge dimers removes the metallicity of the $N = 3p + 2$ family of ribbons.[20]

In order to analyze the influence of such effects on the electronic properties of AGNRs, we have carried out TB calculations for a range of different potential and strain configurations and present representative cases in Figure 5. Panels (a−c) show results for the unperturbed ribbon, with all calculations using up to third nearest-neighbor (3NN) terms in the Hamiltonian. The band structure in Figure 5a is in excellent agreement with that of the H-passivated ribbon examined using DFTB calculations in Figure 4a. Panel (b) shows how the local density of states evolves across the ribbon width, analogously to the result for Si-passivated ribbons in Figure 4f, once a local 6-atom average is applied to remove short-ranged oscillations. It is clear that the gap is uniform across the ribbon, as confirmed by the red curve in panel (c). We note that atom-to-atom fluctuations in the gap width, shown by the gray points here, are unlikely to be resolved in experiment.

Figure 5d−f shows the corresponding band structure, LDOS curves, and gap dependence for an AGNR with an asymmetric potential profile applied, as shown in the inset of panel (d). Although a small decrease in the overall gap is observed, this is uniform across the ribbon. Similar results are found for symmetric, nonlinear, or sublattice-dependent potential profiles, suggesting that local variation of the on-site energy is not sufficient to explain our experimental results. Similarly, in panels (g−i) we consider the effect of a strain near the edges of the ribbon. This is modeled as a Gaussian height deformation placed at each edge, as shown in the inset of Figure 5g, which corresponds to a maximum local strain of ∼4%. In agreement with previous studies, the band gap is considerably lowered. Nevertheless, although the strain is primarily applied to the edges, the band gap is reduced across the entire ribbon once atomic-level fluctuations are averaged out.

CONCLUSIONS

We have shown here high-resolution STM and STS data from epitaxial AGNR structures. Due to the special growth procedure, the ribbons are terminated by the BL, which in turn interacts with the Si atoms of the SiC. The bandgaps measured at the center of the AGNRs fit nicely to expectations for freestanding ribbons, which demonstrates that the SiC substrate plays only a minor role. In contrast to free-stranded ribbons with suspended edges, our structures show a variation of the bandgap. Toward the edge, the value decreases by about a factor of 2. This phenomenon seems to be universal and could be confirmed by the DFTB calculations. It was shown that our bond effectively corresponds to that of a Si termination, which induces a strongly decreasing edge state toward the center of the ribbon. Although the Si-passivation takes place via the nanobuffer stripes, the simplified passivation model used in the calculations explains our findings reasonably.Changes in on-site energies due to charge transfer upon passivation play only a minor rule. As we have explicitly confirmed by calculations, the bandgap variation cannot be explained by the effects of strain or electric fields. Our results have shown that the termination of the edges plays an important role and, e.g., can significantly influence lower subthreshold slopes for possible MOSFET applications.

MATERIALS AND METHODS

Epitaxial armchair graphene nanoribbons were grown on predefined mesa structures on n-doped 6H-SiC(0001) wafers (purchased from SiCrystal GmbH). First, hydrogen etching was applied to flatten the SiC-substrates. Mesa structures along the $\langle 11\bar{2}0\rangle$-direction were defined by means of e-beam lithography using CSAR62 as resist, wet chemical treatments, and subsequent reactive ion etching. These structures of around 150 nm in width and 20 nm in height were observed at elevated temperatures, and AGNRs were selectively

https://doi.org/10.1021/acsnano.3c06449
ACS Nano 2023, 17, 20345−20352

grown on the facets. The samples were inductively heated in a graphite crucible at 1800 °C under an argon atmosphere of 850 mbar. More details are outlined in refs.[5,8,25]

The topography and electronic properties of the AGNRs were investigated by means of low-temperature scanning tunneling microscopy (LT-STM, Omicron) at 80 K using liquid nitrogen. The scanning tunneling spectroscopy (STS) spectra were recorded via a standard lock-in technique (20 meV, 1500 Hz). The samples were degassed at 800 K for some hours under ultrahigh vacuum (UHV) before measurement.

The low-energy electronic band structures of graphene systems are generally well-described using tight-binding (TB) Hamiltonians of the following form.

$$\mathcal{H} = \sum_i \epsilon_i c_i^\dagger c_i + \sum_{\langle i,j \rangle} t_{ij} c_i^\dagger c_j \quad (1)$$

Here, the $c_i^\dagger$ (c_i) operator creates (annihilates) an electron in the p_z orbital at atomic site i, ϵ_i is the on-site energy of an electron occupying an orbital at site i, and t_{ij} is the hopping amplitude between orbitals at sites i and j. Thereby, the TB calculations in this work keep up to third nearest-neighbor (3NN) terms.[40,41] These additional terms are necessary to capture the energy gap behavior reported for AGNRs by ab initio[20] and experimental[42] studies.

Modifications to individual hopping (t_{ij}) or on-site energy (ϵ_i) terms in the TB Hamiltonian allow for the effects of local strains[36] or potentials[7,8] to be included. In this work, we consider the effects of nonuniform strain and local electric fields on the local and global band gaps of AGNRs through the example of Gaussian height profiles and linearly varying potential terms added near the ribbon edges.

While TB simulations can account for a range of different environmental effects in AGNRs, they cannot easily account for passivation scenarios that break the p_z character of the low-energy electronic states. Indeed, TB models implicitly saturate the dangling bonds present at edge carbon atoms. This means that, although no passivation species is specified, nanoribbon band structures calculated using TB models are in better agreement with those of hydrogen-passivated structures than with their unpassivated counterparts.[34,35,43] To examine the role of different edge passivations on the band structure of AGNRs, we employ density functional based tight-binding (DFTB) simulations[44−46] as implemented using the open-source DFTB+ package.[47,48] This is effectively a simplification of density functional theory to a TB-like form and allows for greater accuracy than TB methods at a much reduced computational cost as compared to ab initio simulations. It has previously been applied to model both the growth[49] and electronic properties[31] of graphene/SiC systems.

AUTHOR INFORMATION

Corresponding Authors

Stephen R. Power − *School of Physical Sciences, Dublin City University, 9 Dublin, Ireland*; Email: stephen.r.power@dcu.ie

Christoph Tegenkamp − *Institut für Physik, Technische Universität Chemnitz, 09126 Chemnitz, Germany*; orcid.org/0000-0003-0453-0765; Email: christoph.tegenkamp@physik.tu-chemnitz.de

Authors

Thi Thuy Nhung Nguyen − *Institut für Physik, Technische Universität Chemnitz, 09126 Chemnitz, Germany*

Hrag Karakachian − *Max Planck Institute for Solid State Research, 70569 Stuttgart, Germany*

Ulrich Starke − *Max Planck Institute for Solid State Research, 70569 Stuttgart, Germany*; orcid.org/0000-0003-1153-1862

Complete contact information is available at: https://pubs.acs.org/10.1021/acsnano.3c06449

Notes

The authors declare no competing financial interest.

ACKNOWLEDGMENTS

We would like to thank Ulrike Waizmann and Thomas Reindl for performing the e-beam lithography and reactive ion etching at the Nanostructuring Lab of the Max Planck Institute for Solid State Research. This work was supported by the Deutsche Forschungsgemeinschaft (DFG) through Te386/22-1 within FOR5242, Sta315/9-1, and by the Irish Research Council under the Laureate awards program.

REFERENCES

(1) Wang, H.; Wang, H. S.; Ma, C.; Chen, L.; Jiang, C.; Chen, C.; Xie, X.; Li, A.-P.; Wang, X. Graphene nanoribbons for quantum electronics. *Nature Reviews Physics* **2021**, *3*, 791−802.

(2) Frank, S.; Poncharal, P.; Wang, Z. L.; Heer, W. A. d. Carbon Nanotube Quantum Resistors. *Science* **1998**, *280*, 1744−1746.

(3) Javey, A.; Guo, J.; Wang, Q.; Lundstrom, M.; Dai, H. Ballistic carbon nanotube field-effect transistors. *Nature* **2003**, *424*, 654−657.

(4) Islam, A. E.; Rogers, J. A.; Alam, M. A. Recent Progress in Obtaining Semiconducting Single-Walled Carbon Nanotubes for Transistor Applications. *Adv. Mater.* **2015**, *27*, 7908−7937.

(5) Baringhaus, J.; Ruan, M.; Edler, F.; Tejeda, A.; Sicot, M.; Taleb-Ibrahimi, A.; Li, A.-P.; Jiang, Z.; Conrad, E. H.; Berger, C.; Tegenkamp, C.; de Heer, W. A. Exceptional ballistic transport in epitaxial graphene nanoribbons. *Nature* **2014**, *506*, 349−354.

(6) Miettinen, A. L.; Nevius, M. S.; Ko, W.; Kolmer, M.; Li, A.-P.; Nair, M. N.; Kierren, B.; Moreau, L.; Conrad, E. H.; Tejeda, A. Edge states and ballistic transport in zigzag graphene ribbons: The role of SiC polytypes. *Phys. Rev. B* **2019**, *100*, No. 045425.

(7) Aprojanz, J.; Power, S. R.; Bampoulis, P.; Roche, S.; Jauho, A.-P.; Zandvliet, H. J. W.; Zakharov, A. A.; Tegenkamp, C. Ballistic tracks in graphene nanoribbons. *Nat. Commun.* **2018**, *9*, 4426.

(8) Karakachian, H.; Nguyen, T. T. N.; Aprojanz, J.; Zakharov, A. A.; Yakimova, R.; Rosenzweig, P.; Polley, C. M.; Balasubramanian, T.; Tegenkamp, C.; Power, S. R.; Starke, U. One-dimensional confinement and width-dependent bandgap formation in epitaxial graphene nanoribbons. *Nat. Commun.* **2020**, *11*, 6380.

(9) Acik, M.; Chabal, Y. J. Nature of Graphene Edges: A Review. *Jpn. J. Appl. Phys.* **2011**, *50*, No. 070101.

(10) Cao, T.; Zhao, F.; Louie, S. G. Topological Phases in Graphene Nanoribbons: Junction States, Spin Centers, and Quantum Spin Chains. *Phys. Rev. Lett.* **2017**, *119*, No. 076401.

(11) Gröning, O.; Wang, S.; Yao, X.; Pignedoli, C. A.; Borin Barin, G.; Daniels, C.; Cupo, A.; Meunier, V.; Feng, X.; Narita, A.; Müllen, K.; Ruffieux, P.; Fasel, R. Engineering of robust topological quantum phases in graphene nanoribbons. *Nature* **2018**, *560*, 209−213.

(12) Cai, J.; Ruffieux, P.; Jaafar, R.; Bieri, M.; Braun, T.; Blankenburg, S.; Muoth, M.; Seitsonen, A. P.; Saleh, M.; Feng, X.; Müllen, K.; Fasel, R. Atomically precise bottom-up fabrication of graphene nanoribbons. *Nature* **2010**, *466*, 470−473.

(13) Nguyen, G. D.; et al. Atomically precise graphene nanoribbon heterojunctions from a single molecular precursor. *Nat. Nanotechnol.* **2017**, *12*, 1077−1082.

(14) Talirz, L.; Ruffieux, P.; Fasel, R. On-Surface Synthesis of Atomically Precise Graphene Nanoribbons. *Adv. Mater.* **2016**, *28*, 6222−6231.

(15) Talirz, L.; et al. On-Surface Synthesis and Characterization of 9-Atom Wide Armchair Graphene Nanoribbons. *ACS Nano* **2017**, *11*, 1380−1388.

(16) Chen, S.; Han, Y.; Kolmer, M.; Hall, J.; Hupalo, M.; Evans, J. W.; Tringides, M. C. Targeted Dy intercalation under graphene/SiC for tuning its electronic band structure. *Phys. Rev. B* **2023**, *107*, No. 045408.

(17) Kolmer, M.; Schrunk, B.; Hupalo, M.; Hall, J.; Chen, S.; Zhang, J.; Wang, C.-Z.; Kaminski, A.; Tringides, M. C. Highly Asymmetric Graphene Layer Doping and Band Structure Manipulation in Rare

Earth-Graphene Heterostructure by Targeted Bonding of the Intercalated Gadolinium. *J. Phys. Chem. C* **2022**, *126*, 6863−6873.
(18) Rosenzweig, P.; Karakachian, H.; Link, S.; Küster, K.; Starke, U. Tuning the doping level of graphene in the vicinity of the Van Hove singularity via ytterbium intercalation. *Phys. Rev. B* **2019**, *100*, No. 035445.
(19) Schädlich, P.; et al. Domain Boundary Formation Within an Intercalated Pb Monolayer Featuring Charge-Neutral Epitaxial Graphene. *Advanced Materials Interfaces* **2023**, *10*, No. 2300471.
(20) Son, Y.-W.; Cohen, M. L.; Louie, S. G. Energy Gaps in Graphene Nanoribbons. *Phys. Rev. Lett.* **2006**, *97*, No. 216803.
(21) Ma, C.; Xiao, Z.; Puretzky, A. A.; Wang, H.; Mohsin, A.; Huang, J.; Liang, L.; Luo, Y.; Lawrie, B. J.; Gu, G.; Lu, W.; Hong, K.; Bernholc, J.; Li, A.-P. Engineering Edge States of Graphene Nanoribbons for Narrow-Band Photoluminescence. *ACS Nano* **2020**, *14*, 5090−5098.
(22) Ruffieux, P.; Wang, S.; Yang, B.; Sánchez-Sánchez, C.; Liu, J.; Dienel, T.; Talirz, L.; Shinde, P.; Pignedoli, C. A.; Passerone, D.; Dumslaff, T.; Feng, X.; Müllen, K.; Fasel, R. On-surface synthesis of graphene nanoribbons with zigzag edge topology. *Nature* **2016**, *531*, 489−492.
(23) Keerthi, A.; Radha, B.; Rizzo, D.; Lu, H.; Diez Cabanes, V.; Hou, I. C.-Y.; Beljonne, D.; Cornil, J.; Casiraghi, C.; Baumgarten, M.; Müllen, K.; Narita, A. Edge Functionalization of Structurally Defined Graphene Nanoribbons for Modulating the Self-Assembled Structures. *J. Am. Chem. Soc.* **2017**, *139*, 16454−16457.
(24) Sprinkle, M.; Ruan, M.; Hu, Y.; Hankinson, J.; Rubio-Roy, M.; Zhang, B.; Wu, X.; Berger, C.; de Heer, W. A. Scalable templated growth of graphene nanoribbons on SiC. *Nat. Nanotechnol.* **2010**, *5*, 727−731.
(25) Zakharov, A. A.; Vinogradov, N. A.; Aprojanz, J.; Nguyen, T. T. N.; Tegenkamp, C.; Struzzi, C.; Iakimov, T.; Yakimova, R.; Jokubavicius, V. Wafer Scale Growth and Characterization of Edge Specific Graphene Nanoribbons for Nanoelectronics. *ACS Applied Nano Materials* **2019**, *2*, 156−162.
(26) Palacio, I.; Celis, A.; Nair, M. N.; Gloter, A.; Zobelli, A.; Sicot, M.; Malterre, D.; Nevius, M. S.; de Heer, W. A.; Berger, C.; Conrad, E. H.; Taleb-Ibrahimi, A.; Tejeda, A. Atomic Structure of Epitaxial Graphene Sidewall Nanoribbons: Flat Graphene, Miniribbons, and the Confinement Gap. *Nano Lett.* **2015**, *15*, 182−189.
(27) Nguyen, T. T. N.; de Vries, N.; Karakachian, H.; Gruschwitz, M.; Aprojanz, J.; Zakharov, A. A.; Polley, C.; Balasubramanian, T.; Starke, U.; Flipse, C. F. J.; Tegenkamp, C. Topological Surface State in Epitaxial Zigzag Graphene Nanoribbons. *Nano Lett.* **2021**, *21*, 2876−2882.
(28) Emtsev, K. V.; Speck, F.; Seyller, T.; Ley, L.; Riley, J. D. Interaction, growth, and ordering of epitaxial graphene on SiC(0001) surfaces: A comparative photoelectron spectroscopy study. *Phys. Rev. B* **2008**, *77*, No. 155303.
(29) Merino-Díez, N.; Garcia-Lekue, A.; Carbonell-Sanromà, E.; Li, J.; Corso, M.; Colazzo, L.; Sedona, F.; Sánchez-Portal, D.; Pascual, J. I.; de Oteyza, D. G. Width-Dependent Band Gap in Armchair Graphene Nanoribbons Reveals Fermi Level Pinning on Au(111). *ACS Nano* **2017**, *11*, 11661−11668.
(30) Baringhaus, J.; Aprojanz, J.; Wiegand, J.; Laube, D.; Halbauer, M.; Hübner, J.; Oestreich, M.; Tegenkamp, C. Growth and characterization of sidewall graphene nanoribbons. *Appl. Phys. Lett.* **2015**, *106*, No. 043109.
(31) N Nair, M.; Palacio, I.; Celis, A.; Zobelli, A.; Gloter, A.; Kubsky, S.; Turmaud, J.-P.; Conrad, M.; Berger, C.; de Heer, W.; et al. Band gap opening induced by the structural periodicity in epitaxial graphene buffer layer. *Nano Lett.* **2017**, *17*, 2681−2689.
(32) Sun, L.; Li, Q.; Ren, H.; Su, H.; Shi, Q. W.; Yang, J. Strain effect on electronic structures of graphene nanoribbons: A first-principles study. *J. Chem. Phys.* **2008**, *129*, No. 074704.
(33) Power, S. R.; Ferreira, M. S. Indirect Exchange and Ruderman−Kittel−Kasuya−Yosida (RKKY) Interactions in Magnetically-Doped Graphene. *Crystals* **2013**, *3*, 49−78.
(34) Ma, F.; Guo, Z.; Xu, K.; Chu, P. K. First-principle study of energy band structure of armchair graphene nanoribbons. *Solid state communications* **2012**, *152*, 1089−1093.
(35) Raza, H. Edge and passivation effects in armchair graphene nanoribbons. *Phys. Rev. B* **2011**, *84*, No. 165425.
(36) Pereira, V. M.; Castro Neto, A. H.; Peres, N. M. R. Tight-binding approach to uniaxial strain in graphene. *Phys. Rev. B* **2009**, *80*, No. 045401.
(37) Mammadov, S.; Ristein, J.; Krone, J.; Raidel, C.; Wanke, M.; Wiesmann, V.; Speck, F.; Seyller, T. Work function of graphene multilayers on SiC(0001). *2D Materials* **2017**, *4*, No. 015043.
(38) Raza, H.; Kan, E. C. Armchair graphene nanoribbons: Electronic structure and electric-field modulation. *Phys. Rev. B* **2008**, *77*, No. 245434.
(39) Peng, X.; Velasquez, S. Strain modulated band gap of edge passivated armchair graphene nanoribbons. *Appl. Phys. Lett.* **2011**, *98*, No. 023112.
(40) Gunlycke, D.; White, C. T. Tight-binding energy dispersions of armchair-edge graphene nanostrips. *Phys. Rev. B* **2008**, *77*, No. 115116.
(41) Hancock, Y.; Uppstu, A.; Saloriutta, K.; Harju, A.; Puska, M. J. Generalized tight-binding transport model for graphene nanoribbon-based systems. *Phys. Rev. B* **2010**, *81*, No. 245402.
(42) Wang, W.-X.; Zhou, M.; Li, X.; Li, S.-Y.; Wu, X.; Duan, W.; He, L. Energy gaps of atomically precise armchair graphene sidewall nanoribbons. *Phys. Rev. B* **2016**, *93*, No. 241403.
(43) Raza, H.; Kan, E. C. An extended Hückel theory based atomistic model for graphene nanoelectronics. *Journal of Computational Electronics* **2008**, *7*, 372−375.
(44) Seifert, G.; Porezag, D.; Frauenheim, T. Calculations of molecules, clusters, and solids with a simplified LCAO-DFT-LDA scheme. *International journal of quantum chemistry* **1996**, *58*, 185−192.
(45) Porezag, D.; Frauenheim, T.; Köhler, T.; Seifert, G.; Kaschner, R. Construction of tight-binding-like potentials on the basis of density-functional theory: Application to carbon. *Phys. Rev. B* **1995**, *51*, 12947−12957.
(46) Elstner, M.; Porezag, D.; Jungnickel, G.; Elsner, J.; Haugk, M.; Frauenheim, T.; Suhai, S.; Seifert, G. Self-consistent-charge density-functional tight-binding method for simulations of complex materials properties. *Phys. Rev. B* **1998**, *58*, 7260−7268.
(47) Hourahine, B.; Aradi, B.; Blum, V.; Bonafé, F.; Buccheri, A.; Camacho, C.; Cevallos, C.; Deshaye, M.; Dumitrica, T.; Dominguez, A.; et al. DFTB+, a software package for efficient approximate density functional theory based atomistic simulations. *J. Chem. Phys.* **2020**, *152*, No. 124101.
(48) Rauls, E.; Elsner, J.; Gutierrez, R.; Frauenheim, T. Stoichiometric and non-stoichiometric (1010) and (1120) surfaces in 2H−SiC: A theoretical study. *Solid state communications* **1999**, *111*, 459−464.
(49) Norimatsu, W.; Kusunoki, M. Growth of graphene from SiC(0001) surfaces and its mechanisms. *Semicond. Sci. Technol.* **2014**, *29*, No. 064009.

https://doi.org/10.1021/acsnano.3c06449
ACS Nano 2023, 17, 20345−20352